有機超伝導体と量子スピン液体：κ-$(ET)_2M_2(CN)_3$ (M = Cu, Ag)

齋藤軍治[*1]
吉田幸大[*2]　平松孝章[*2]
大塚晃弘[*3]　前里光彦[*3]
清水康弘[*4]　伊東裕[*4]
中村優斗[*4]　岸田英夫[*4]
渡邉真史[*5]　熊井玲児[*6]

[*]齋藤軍治　客員フェロー

Organic Superconductor and Quantum Spin Liquid: κ-$(ET)_2M_2(CN)_3$ (M = Cu, Ag)

Gunzi SAITO[*1], Yukihiro YOSHIDA[*2], Takaaki HIRAMATSU[*2], Akihiro OTSUKA[*3], Mitsuhiko MAESATO[*3], Yasuhiro SHIMIZU[*4], Hiroshi ITO[*4], Yuto NAKAMURA[*4], Hideo KISHIDA[*4], Masashi WATANABE[*5] and Reiji KUMAI[*6]

The quantum spin liquid (QSL) that originates from the geometrical spin frustration in a triangular magnetic lattice, was proposed theoretically in 1973. In 2003, the first QSL candidate was manifested in a dimer-type Mott insulator, κ-$(ET)_2Cu_2(CN)_3$ (**1**), where ET is an electron donor, bis(ethylenedithio) tetrathiafulvalene and $[Cu_2(CN)_3^-]_\infty$ is a two-dimensional polyanion. Based on the key–keyhole strategy, i.e., the geometrical relation between $(ET)_2^{\bullet+}$ with a single spin site and an anion opening in $[Cu_2(CN)_3^-]_\infty$, a new QSL candidate, κ-$(ET)_2Ag_2(CN)_3$ (**2**), with different key–keyhole relation was prepared. Similar to **1**, salt **2** with a nearly equilateral triangular magnetic lattice and strong electron correlation demonstrates a superconducting state next to the QSL state under pressure. However, the different key–keyhole relation leads to a higher superconducting critical temperature and a more robust QSL state over a wider pressure range compared to **1**.

1. Introduction

Spin-frustrated materials based on geometrically localised spins[1,2] have been of great interest to materials scientists because a conventional long-range magnetic ordering is suppressed, resulting in a novel quantum spin liquid (QSL) state[2]. The QSL state is thought to have a ground state comprising many degenerate states[1]. Thus, such a system retains finite entropy even at absolute zero temperature. To construct such a frustrated system, as an example, a triangular magnetic lattice (TML) geometry (Fig. 1a)[3,4] subject to contradictory constraints is necessary, where the direction of the third spin having antiferromagnetic (AF) exchange interactions is not determined a priori among the three spins.

The first QSL candidate, κ-$(ET)_2Cu_2(CN)_3$ (**1**, ET = bis (ethylenedithio)tetrathiafulvalene; Fig. 1b)[5], is a dimer-type Mott insulator in which $(ET)_2^{\bullet+}$ has an S = 1/2 spin and $[Cu_2(CN)_3^-]_\infty$ is a diamagnetic polymeric anion. Salt **1** has strong electron correlation, as indicated by U/W = 0.93, which is close to the Mott boundary, $U \approx W$[6], where U and W are the on-site Coulomb repulsion energy and bandwidth, respectively. The localised spins on $(ET)_2^{\bullet+}$ form a nearly equilateral TML in terms of the interdimer transfer integrals, t'/t (= 1.09), as shown in Fig. 1c, and the QSL state was confirmed experimentally down to 20 mK[7]. Under pressure[8–10], a superconducting (SC) state appears next to the QSL state. ^{13}C NMR

2017年3月2日 受理
*1 豊田理化学研究所客員フェロー
名城大学教授
京都大学名誉教授，理学博士
専門分野：材料科学，有機物性化学，有機機能性材料の開発研究
*2 名城大学
*3 京都大学
*4 名古屋大学
*5 東北大学
*6 高エネルギー加速器研究機構

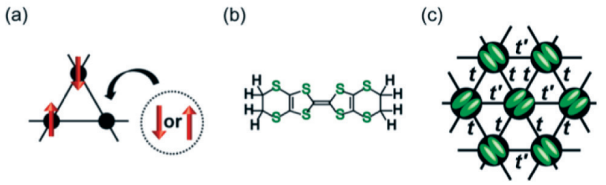

Fig. 1 (a) Triangular spin geometry exhibiting strong spin frustration, where red arrows indicate the spin.
(b) ET molecular structure.
(c) A schematic of the triangular magnetic lattice of dimer-type Mott insulators, κ-(ET)$_2$X (X: monoanion). Green ellipsoids indicate ET molecules viewed along the molecular long axis, and black circles represent ET dimers with single spin sites. The ratio t'/t represents the shape of the isosceles triangular magnetic lattice, where t and t' are interdimer transfer integrals.

measurements (^{13}C enriched at the central C=C bond of ET) under pressure strongly suggest *d*-wave SC symmetry[11]. Thus, **1** exhibits a competition between the localised, frustrated, itinerant and exotic pairing of spins[12].

Since the discovery of the QSL state in **1**, several QSL candidates based on triangular or kagome lattices have been reported[4,13–17]. Notably, except for **1**, none of the QSL candidates reported thus far exhibit SC behaviour. Here, we report another QSL candidate recently obtained, κ-(ET)$_2$Ag$_2$(CN)$_3$ (**2**)[18], with a higher SC critical temperature T_c (5.2 K) and a robust QSL state with a higher SC critical pressure P_c (1.05 GPa) compared to those for **1** (T_c = 3.9 K, P_c = 0.36 GPa)[10].

2. Results and Discussion

Single crystals of **2** were prepared by galvanostatic electrooxidation of ET. The temperature dependence of the lattice parameters and the anion structures clearly show no structural phase transitions or static charge disproportionation of ET in the investigated temperature range (8 K–RT). First we describe guiding principles for QSL materials with a nearby SC state for dimer-type ET solids, κ-(ET)$_2$X (X: monoanion)[19]. We observed that the planar tridentate coordination of diamagnetic Cu(I) ions in $[Cu_2(CN)_3^-]_\infty$ is the main driving force for the two-dimensional (2D) TML composed of partially charged $(ET)_2^{\bullet+}$ in **1**. The planar polymeric anion, $[Cu_2(CN)_3^-]_\infty$, has openings, and the arrangement of the anion openings is triangular because of the planar tridentate coordination of Cu(I) ions (Fig.2a). The geometrical fit between a spin site $(ET)_2^{\bullet+}$ and the anion opening results in a TML

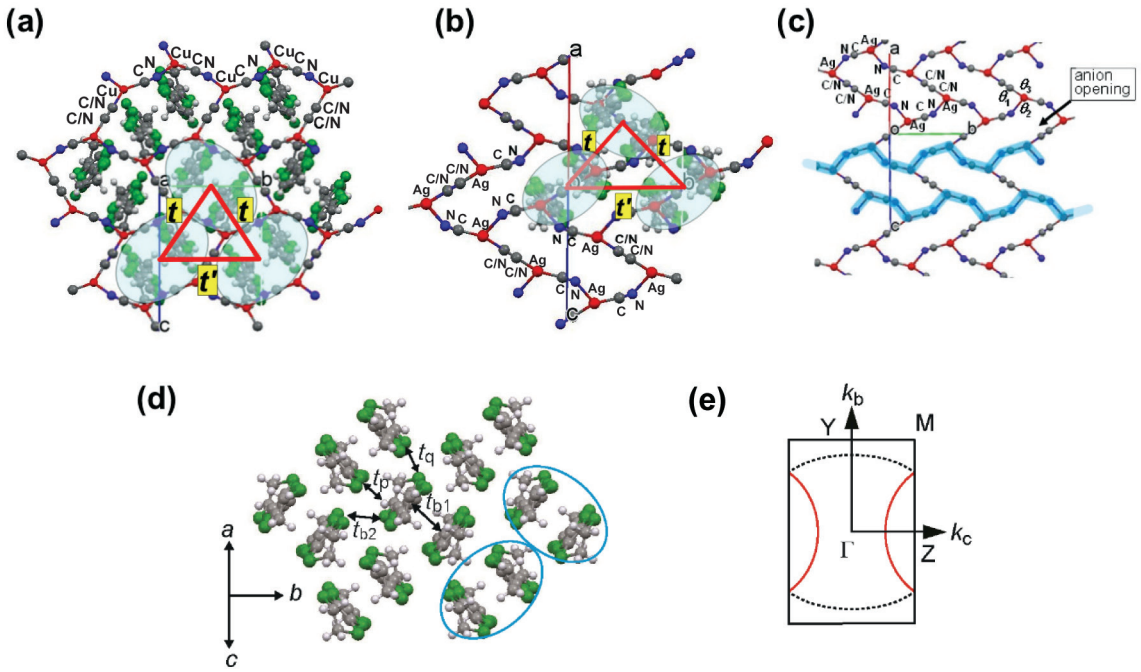

Fig. 2 (a) Crystal structure of **1** viewed along the *a* axis.
(b) Crystal structure of **2** viewed along the [101] direction. Red triangles in (a) and (b) are the triangular magnetic lattice.
(c) Infinite zigzag chains of –Ag–CN–Ag–CN– or –Ag–NC–Ag–NC– along the *b* axis (two chains are represented by blue thick lines) are connected by disordered CN (indicated by C/N) groups along the *c* axis to form an anion opening. θ_1, θ_2 and θ_3 are the coordination angles around the Ag(I) ion.
(d) Projected view of ET molecules along the molecular long axis for **2** with transfer interactions (t_{b1}, t_{b2}, t_p and t_q) at RT, where $U = 2|t_{b1}|$, $t' = |t_{b2}|/2$ and $t = (|t_p| + |t_q|)/2$. The pair of blue ellipsoids correspond to two orthogonal ET dimers $(ET)_2^{\bullet+}$.
(e) Calculated Fermi surface of **2** at RT. Black dotted and red solid lines indicate 1D electron-like and 2D cylindrical hole-like Fermi surfaces, respectively. The following color scheme is employed.
H: light grey, C: grey, N: blue, S: green, Cu and Ag: red.

according to a key–keyhole relation, where the key is the spin site $(ET)_2^{\bullet+}$ and the hole is the anion opening. To realize a QSL state, the band parameters U and W (hence U/W) and t'/t are tuned by the kind of transition metal, the sizes and shapes of ligands and the connectivity of ligands to central metals. Then we adjust intentionally or unintentionally the magnitudes of t'/t and U/W to allocate the spin-frustrated TML near Mott boundary, which may exhibit a competition between the localised, itinerant (metal or SC) and frustrated states. Therefore, a search for partially charged salts having a triangular key–keyhole relation, residing close to the Mott boundary ($U \sim W$) in the insulating side and having strong spin frustration ($t'/t \sim 1$) is the essential guiding principle for QSL materials with a nearby SC state.

Figures 2a and 2b show the layered structures of **1**[9,10,19] and **2**,[18] respectively. The 2D conducting ET layer is sandwiched between the insulating anion layers. The anions $M_2(CN)_3$ (M(I) = Cu, Ag) polymerise, resulting in the formation of a 2D anion network. The infinite zigzag chains along the b axis composed of M(I) and CN^- (–M–CN–M–CN– or –M–NC–M–NC–; two chains are depicted in blue thick lines in Fig. 2c for **2**) are connected by disordered CN^- groups (indicated by C/N) to form anion openings with a rectangular shape for **2** and a hexagonal shape for **1**. The rectangular shape for **2** arises from the T-shaped coordination around Ag(I). The angle θ_3 (160.8°) is very large relative to the other two angles, θ_1 (104.4°) and θ_2 (93.8°), whereas the corresponding angles for **1** are approximately equivalent. The large ionic radius of Ag(I) (1.29 Å for a six-coordinate system[20]) relative to that of Cu(I) (0.91 Å for a six-coordinate system[20]) and the different connectivity of M(I) affords a smaller anion opening area for **2** (19.5 $Å^2$ for **1** vs. 15.8 $Å^2$ for **2**).

ET molecules are arranged in a κ-type packing motif of orthogonal $(ET)_2^{\bullet+}$ dimers (encircled by blue ellipsoids in Fig. 2d). The transfer integrals between ET molecules are calculated on the basis of the extended Hückel calculation[21]; the band parameters for **2**, together with those for **1**[19,22], are summarised in Table 1. Similar ET packing and equivalent crystal symmetry ($P2_1/c$) for **1** and **2** result in similar calculated Fermi surfaces (Fig. 2e for **2**) and energy dispersion.

Table 1 Band parameters by extended Hückel method for κ-$(ET)_2M_2(CN)_3$ (M = Cu (**1**) and Ag (**2**)) at typical temperatures

M	T / K	t' / meV	t / meV	t'/t	U / meV	W / meV	U/W
Cu (**1**)[19,22]	300	57.4	52.6	1.091	449	483	0.929
	100	56.8	52.9	1.074	483	480	1.005
	5	59.0	53.1	1.111	499	487	1.025
Ag (**2**)	300	49.0	50.6	0.967	465	446	1.043
	100	48.8	53.5	0.913	518	460	1.126
	8	49.0	54.2	0.903	535	465	1.151

Even though both **1** and **2** have similar alternate stacking of ET layers and anion layers (//a), the relative orientation between the anion opening and $(ET)_2^{\bullet+}$ differs substantially in each salt. Figures 2a and 2b clearly show the formation of TML drawn in red for the transfer interactions, t (= ($|t_p| + |t_q|$) / 2) and t' (= $|t_{b2}|$ / 2), derived from the geometrical fit using the key–keyhole relation that gives the ratio t'/t = 1.09 for **1** and 0.97 for **2**. The key–keyhole relation in **1** is characterized as key-on-hole type when viewed along the a axis where the neighbouring polymerized anions are eclipsed. Such a relation is commonly observed for SC salts κ-$(ET)_2CuL_1L_2$, in which the ligand L_1 links Cu(I) to form infinite zigzag chains whereas the ligand L_2 attaches to Cu(I) as a pendant ligand or connects the infinite chains (CuL_1L_2 = $Cu(NCS)_2$[23], $Cu[N(CN)_2]Cl$[24], $Cu[N(CN)_2]Br$[25], $Cu[N(CN)_2]I$[26], and $Cu(CN)[N(CN)_2]$[27]). Similar relation was also found for the recently reported Ag(I)-containing SC salt κ-$(ET)_2Ag(CN)[N(CN)_2]$ with T-shaped connectivity[28].

For **2**, the key–keyhole relation is different from that of **1**. When viewed through the eclipsed polymerized anions, the ET dimers in **2** are not located on the anion opening, but on the top of the rim of the anion opening near the disordered cyano group (Fig. 2b). Although the key-on-rim type key–keyhole relation in **2** differs from the key-on-hole relations in κ-$(ET)_2CuL_1L_2$ and κ-$(ET)_2Ag(CN)[N(CN)_2]$, the geometrical pattern of the anion openings apparently serves as a template for the TML. The difference in the key–keyhole relation results in the difference in band parameters, W, U, and density of states at the Fermi level $D(\varepsilon_F)$, between **1** and **2**. Before that, the temperature dependences t'/t and U/W are discussed to clarify the reason why **1** and **2** keep the strong spin frustration and electron correlation down to low temperatures, in contrast to those of other κ-$(ET)_2X$.

The temperature dependence of t'/t (Fig. 3a) is related to the thermal changes in the crystal lattice and is therefore partly explainable by the kinds, shape and packing pattern of the anion species. κ-$(ET)_2X$ salts having 1D infinite anionic zigzag chains such as X = $Cu(NCS)_2$, $Cu[N(CN)_2]Cl$, $Cu[N(CN)_2]Br$, $Cu(CN)[N(CN)_2]$, and $Ag(CN)[N(CN)_2]$ exhibit little temperature dependence of t'/t down to 100 K ($|\Delta t'/t| < 10\%$), because of the weak anisotropy in lattice elasticity of the polymeric anion layers. In contrast, κ-$(ET)_2X$ salts with bulky non-planar discrete anions such as X = CF_3SO_3 (t'/t = 1.79)[31] and $B(CN)_4$ (t'/t = 1.42)[32] give large t'/t values and exhibit significant temperature dependences. For the TML of **1** and **2**, their geometries remain highly frustrated down to low

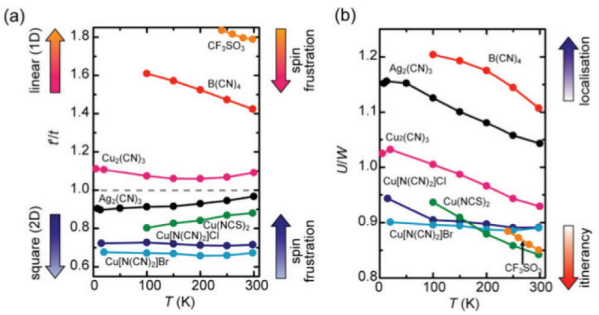

Fig. 3 Temperature dependence of (a) t'/t and (b) U/W for **1** and **2** compared with those of AF salts X = Cu[N(CN)$_2$]Cl (T_N = 27 K and T_c = 12.8 K at 0.03 GPa)[24, 33, 34] and CF_3SO_3 (T_N = 2.5 K and T_c = 4.8 K at 1.3 GPa)[31], SC salts X = Cu(NCS)$_2$ (T_c = 10.4 K)[23], Cu[N(CN)$_2$]Br (T_c = 11.8 K)[25] and a valence bond solid X = B(CN)$_4$[32], where T_N is the Néel temperature. For (a), the spin lattice forms a 2D square lattice in the smaller t'/t region and a 1D linear lattice in larger t'/t regions. Spin frustration is expected to maximize at t'/t = 1. For (b), the electron correlation, U/W, increases at low temperatures in all of the salts. The low temperature data below 100 K were calculated based on the crystal structure reported by other laboratories for X = Cu[N(CN)$_2$]Cl[29], Cu[N(CN)$_2$]Br[30], and Cu$_2$(CN)$_3$[22].

temperatures (t'/t = 1.09–1.11 for RT–5 K for **1** and 0.97–0.90 for RT–8 K for **2**), giving rise to a stable QSL state.

Salts with the aforementioned polymeric anions have distorted isosceles with $t'/t \leq 0.88$[19] approaching a 2D square magnetic lattice, whereas salts with bulky non-planar discrete anions also have distorted isosceles but with $t'/t > 1.4$ approaching a 1D linear magnetic lattice. Both t'/t values deviate from the highly spin-frustrated regime, i.e., κ-(ET)$_2$Cu[N(CN)]$_2$Cl with a small t'/t (0.72) and κ-(ET)$_2$CF$_3$SO$_3$ with a large t'/t undergo a long-range AF ordering at 27 K[33, 34] and 2.5 K[31], respectively. In the case of κ-(ET)$_2$B(CN)$_4$, the spin frustration is not substantial; however, the moderate frustration may be responsible for a phase transition from a QSL state to a spin-singlet valence bond solid state at 5 K[32].

We next examine the structural parameters characterising W, U and U/W to control the Mott boundary and $D(\varepsilon_F)$. Compared with **1**, the smaller anion opening in **2** would result in a larger W since the larger t and t' are expected. However, in fact, the W for **2** is smaller than that for **1**. The less dense packing of $(ET)_2^{\bullet+}$ in **2** owing to the key-on-rim type key–keyhole relation, which provides considerably smaller t' than those for the key-on-hole type **1** (Table 1), is responsible for the smaller W. The anion layer area, defined as the unit area in the bc plane, is a good structural parameter to assess the packing density of $(ET)_2^{\bullet+}$. The anion layer area of **2** (116.7 Å^2) is a little larger than that of **1** (115.0 Å^2), indicating a slightly looser packing of $(ET)_2^{\bullet+}$ in **2**. Therefore, the W of **2** is slightly smaller and the U of **2** is slightly larger than those of **1** down to low temperatures (Table 1), that suggest that the $D(\varepsilon_F)$ and hence the T_c of **2** will be higher than those of **1**. Actually, a small but significant difference exists in the calculated $D(\varepsilon_F)$ value at low temperatures between **1** (1.06 states eV^{-1} spin^{-1} at 5 K) and **2** (1.18 states eV^{-1} spin^{-1} at 8 K).

Figure 3b shows the temperature dependence of U/W to examine the Mott boundary in κ-(ET)$_2$X. In general, κ-(ET)$_2$X salts presented in this paper exhibit an increase in U/W to some extent upon cooling (≤11.3% down to 100 K) mainly because of an increase in dimerization energy. The magnitude of the increase in U/W is variable among the salts and is mainly ascribed to the temperature dependence of U, and that is related with the temperature dependence of geometries of ET dimer since $U = 2|t_{b1}|$ within the dimer model approximation[35]. Salts **1** and **2** exhibit a similar and considerable increase in U/W associated with an increase in U by 7.6–11.4% and temperature-insensitive W down to 100 K. Such a remarkable enhancement of U/W was also observed for X = Cu(NCS)$_2$ and B(CN)$_4$ for the same reason (8.8–11.3% down to 100 K). In contrast, the salts X = Ag(CN)[N(CN)$_2$], Cu(CN)[N(CN)$_2$], Cu[N(CN)$_2$]Br, and Cu[N(CN)$_2$]Cl exhibit a slight increase in U/W down to 100 K (≤ 5.7%). Within our extended Hückel calculations, a boundary between localisation (Mott insulators such as X = CF_3SO_3, Cu[N(CN)$_2$]Cl, Cu$_2$(CN)$_3$, Ag$_2$(CN)$_3$, and B(CN)$_4$) and itinerancy (metals such as X = Ag(CN)[N(CN)$_2$], Cu(CN)[N(CN)$_2$], Cu(NCS)$_2$, and Cu[N(CN)$_2$]Br) is defined at around U/W = 0.94 at low temperature. This value approaches the generally anticipated Mott boundary of $U/W \approx 1$[6], which amounts to a 5.6% increase from the RT value (0.89). Thus, both **1** and **2** maintain strong electron correlation with **2** residing a little far away from the Mott boundary compared with **1** down to less than 10 K (Fig. 3b).

The physical properties of **1** have been reported by us[5, 7, 8, 10–12] and by other groups[9, 13, 22, 36–38], whereas those of **2** were very recently published[18, 39.40]. Here, we describe only the essential issues emphasising that a competition among the localisation and itinerancy of electrons, spin frustration and spin pairing to achieve an SC state is a characteristic feature of QSL candidates **1** and **2**. The ^{1}H NMR data down to 32 mK for **1**[5] and 120 mK for **2**[18] indicate no appearance of an internal magnetic field caused by a long-range AF ordering. The RT static magnetic susceptibility (χ) of **2** (6.4×10^{-4} emu mol^{-1}) is higher than that of **1** (4.7×10^{-4} emu mol^{-1})[5], reflecting the slightly increased U and $D(\varepsilon_F)$ in **2**. The χ value of **2** increases gradually upon cooling, exhibiting a broad peak at approximately 50 K, and then decreases smoothly. On the basis of the Heisenberg triangular AF lattice model[41], the temperature dependence of χ gives the value for the AF exchange interaction, $|J|/k_B$ = 175 K for **2**[18] vs. 250 K for **1**[5],

where J and k_B are the AF exchange interaction and Boltzmann constant, respectively. In addition, **1** and **2** behave as semiconductors with comparable conductivities and activation energies (σ_{RT} = 2 S cm^{-1} and ε_a = 50–88 meV for **2** vs. σ_{RT} = 3–7 *S* cm^{-1} and ε_a = 36–43 meV for **1**)[10], indicating that both salts are closer to the itinerant region than typical dimer-type Mott insulators such as β'-(ET)$_2$ICl$_2$ (U/W = 2.06, $\sigma_{RT} = 3 \times 10^{-2}$ S cm^{-1} and ε_a = 120 meV)[42]. The smaller activation energy of **1** compared with that of **2** suggests that salt **1** more closely approaches the Mott boundary. Similar to **1**, salt **2** undergoes a phase transition from the QSL to metallic state under an applied hydrostatic pressure greater than 0.99 GPa and to the SC state with an onset T_c of 5.2 K at 1.05 GPa[18] vs. onset T_c of 3.9 K at 0.36 GPa for **1**[10]. The phase transition from the QSL to metallic state shows positive pressure dependence, similar to that observed in **1**[43], which confirms residual spin entropy in the QSL state. Relative to **1**, the higher T_c for **2** is consistent with the higher expected $D(\varepsilon_F)$ corresponding to the narrower W for **2**. Notably, the QSL state in **2** covers a wider pressure range by about 0.6 GPa than **1**, because **2** resides far away from the Mott boundary in the localised phase.

In summary, we have prepared a new QSL candidate **2** with the key-on-rim type key–keyhole relation between $(ET)_2^{\bullet+}$ (key) and an anion opening in a diamagnetic 2D polyanion $[Ag_2(CN)_3^-]_\infty$ (keyhole). Such a key–keyhole relation has played a critical role in the development of these systems, because it allows the controllability of spin frustration t'/t and electron correlation U/W via the choice of anion species. This is the practical strategy to develop the TML and eventually QSL system by arranging the magnetic species using the appropriate supramolecular architectures.

ACKNOWLEDGMENT

This work was supported by JSPS KAKENHI Grant Numbers JP23225005 and JP26288035. Thanks are due to the Instrument Center, the Institute for Molecular Science, for the assistance in obtaining the single-crystal diffraction data at 13 and 50 K. The synchrotron X-ray study at 8 K was performed with the approval of the Photon Factory Program Advisory Committee (No.2014S2-001).

References

1) G. H. Wannier, *Phys. Rev.,* **79** (1950) 357-364.
2) P. W. Anderson, *Mater. Res. Bull.,* **8** (1973) 153-160.
3) J. E. Greedan, *J. Mater. Chem.,* **11** (2001) 37-53.
4) L. Balents*, Nature,* **464** (2010) 199-208.
5) Y. Shimizu, K. Miyagawa, K. Kanoda, M. Maesato and G. Saito, *Phys. Rev. Lett.,* **91** (2003) 107001.
6) N. F. Mott*, Metal-Insulator Transitions*, 2nd Edition (Taylor and Francis, 1990).
7) F. L. Pratt, P. J. Baker, S. J. Blundell, T. Lancaster, S. Ohira-Kawamura, C. Baines, Y. Shimizu, K. Kanoda, I. Watanabe and G. Saito*, Nature,* **471** (2011) 612-616.
8) Y. Shimizu, M. Maesato and G. Saito*, J. Phys. Soc. Jpn.,* **80** (2011) 074702.
9) U. Geiser, H. H. Wang, K. D. Carlson, J. M. Williams, H. A. Charlier, J. E. Heindl, G. A. Yaconi, B. J. Love, M. W. Lathrop, J. E. Schirber, D. L. Overmyer, J. Ren and M.-H. Whangbo*, Inorg. Chem.,* **30** (1991) 2586-2588.
10) T. Komatsu, N. Matsukawa, T. Inoue and G. Saito*, J. Phys. Soc. Jpn.,* **65** (1996) 1340-1354.
11) Y. Shimizu, H. Kasahara, T. Furuta, K. Miyagawa, K. Kanoda, M. Maesato and G. Saito, *Phys. Rev. B,* **81** (2010) 224508.
12) G. Saito and Y. Yoshida, *Bull. Chem. Soc. Jpn*., **80** (2007) 1-137.
13) B. J. Powell and R. H. McKenzie, *Rep. Prog. Phys.,* **74** (2011) 056501.
14) T. Isono, H. Kamo, A. Ueda, K. Takahashi, M. Kimata, H. Tajima, S. Tsuchiya, T. Terashima, S. Uji and H. Mori, *Phys. Rev. Lett.,* **112** (2014) 177201.
15) T. Itou, A. Oyamada, S. Maegawa, M. Tamura and R. Kato, *J. Phys.: Condens. Matter*, **19** (2007) 145247.
16) T.-H. Han, J. S. Helton, S. Chu, D. G. Nocera, J. A. Rodriguez-Rivera, C. Broholm and Y. S. Lee*, Nature,* **492** (2012) 406-410.
17) Y. Okamoto, M. Nohara, H. Aruga-Katori and H. Takagi, *Phys. Rev. Lett.,* **99** (2007) 137207.
18) Y. Shimizu, T. Hiramatsu, M. Maesato, A. Otsuka, H. Yamochi, A. Ono, M. Itoh, M. Yoshida, M. Takigawa, Y. Yoshida and G. Saito, *Phys. Rev. Lett.,* **117** (2016) 107203.
19) T. Hiramatsu, Y. Yoshida, G. Saito, A. Otsuka, H. Yamochi, M. Maesato, Y. Shimizu, H. Ito and H. Kishida*, J. Mater. Chem. C*, **3** (2015) 1378-1388.
20) R. D. Shannon, *Acta Crystallogr. A*, **32** (1976) 751-767.
21) T. Mori, A. Kobayashi, Y. Sasaki, H. Kobayashi, G. Saito, and H. Inokuchi, *Bull. Chem. Soc. Jpn*., **57** (1984) 627-633.
22) H. O. Jeschke, M. de Souza, R. Valenti, R. S. Manna, M. Lang and J. A. Schlueter, *Phys. Rev. B,* **85** (2012) 035125.
23) H. Urayama, H. Yamochi, G. Saito, K. Nozawa, T. Sugano, M. Kinoshita, S. Sato, K. Oshima, A. Kawamoto and J. Tanaka, *Chem. Lett*., **17** (1988) 55-58.
24) J. M. Williams, A. M. Kini, H. H. Wang, K. D. Carlson, U. Geiser, L. K. Montgomery, G. J. Pyrka, D. M. Watkins, J. M. Kommers, S. J. Boryschuk, A. V. S. Crouch, W. K. Kwok, J. E. Schirber, D. L. Overmyer, D. Jung and M.-H. Whangbo*, Inorg. Chem.,* **29** (1990) 3272-3274.
25) A. M. Kini, U. Geiser, H. H. Wang, K. D. Carlson, J. M. Williams, W. K. Kwok, K. G. Vandervoort, J. E. Thompson, D. L. Stupka, D. Jung and M.-H. Whangbo*, Inorg. Chem.,* **29** (1990) 2555-2557.

26) N. D. Kushch, M. A. Tanatar, E. B. Yagubskii and T. Ishiguro, *JETP Lett.,* **73** (2001) 429-431.
27) H. Yamochi, T. Nakamura, T. Komatsu, N. Matsukawa, T. Inoue and G. Saito, *Solid State Commun.,* **82** (1992) 101-105.
28) Y. Yoshida, H. Hayama, M. Ishikawa, A. Otsuka, H. Yamochi, Y. Nakamura, H. Kishida, H. Ito, M. Maesato and G. Saito*, J. Phys. Soc. Jpn.,* **84** (2015) 123801.
29) M. Watanabe, Y. Nogami, K. Oshima, H. Ito, T. Ishiguro and G. Saito, *Synth. Met.,* **103** (1999) 1909-1910.
30) U. Geiser, A. M. Kini, H. H. Wang, M. A. Beno and J. M. Williams, *Acta Crystallogr. C,* **47** (1991) 190-192.
31) H. Ito, T. Asai, Y. Shimizu, H. Hayama, Y. Yoshida and G. Saito, *Phys. Rev. B,* **94** (2016) 020503.
32) Y. Yoshida, H. Ito, M. Maesato, Y. Shimizu, H. Hayama, T. Hiramatsu, Y. Nakamura, H. Kishida, T. Koretsune, C. Hotta and G. Saito, *Nature Phys.,* **11** (2015) 679-683.
33) U. Welp, S. Fleshler, W. K. Kwok, G. W. Crabtree, K. D. Carlson, H. H. Wang, U. Geiser, J. M. Williams and V. M. Hitsman, *Phys. Rev. Lett.,* **69** (1992) 840-843.
34) K. Miyagawa, A. Kawamoto, Y. Nakazawa and K. Kanoda, *Phys. Rev. Lett.,* **75** (1995) 1174-1177.
35) A. B. Harris and R. V. Lange, *Phys. Rev.,* **157** (1967) 295-314.
36) R. S. Manna, M. de Souza, A. Brühl, J. A. Schlueter and M. Lang, *Phys. Rev. Lett.,* **104** (2010) 016403.
37) M. Abdel-Jawad, I. Terasaki, T. Sasaki, N. Yoneyama, N. Kobayashi, Y. Uesu and C. Hotta, *Phys. Rev. B,* **82** (2010) 125119.
38) S. Tomić and M. Dressel, *Rep. Prog. Phys.,* **78** (2015) 096501.
39) M. Pinterić, P. Lazić, A. Pustogow, T. Ivek, M. Kuveždić, O. Milat, B. Gumhalter, M. Basletić, M. Čulo, B. Korin-Hamzić, A. Löhle, R. Hübner, M. Sanz Alonso, T. Hiramatsu, Y. Yoshida, G. Saito, M. Dressel and S. Tomić, *Phys. Rev. B,* **94** (2016) 161105.
40) Y. Nakamura, T. Hiramatsu, Y. Yoshida, G. Saito and H. Kishida*, J. Phys. Soc. Jpn.,* **86** (2017) 014710.
41) N. Elstner, R. R. P. Singh and A. P. Young, *Phys. Rev. Lett.,* **71** (1993) 1629-1632.
42) N. Yoneyama, A. Miyazaki, T. Enoki and G. Saito, *Bull. Chem. Soc. Jpn*. **72** (1999) 639-651.
43) Y. Kurosaki, Y. Shimizu, K. Miyagawa, K. Kanoda and G. Saito, *Phys. Rev. Lett.,* **95** (2005) 177001.